Journal of
Computational and Theoretical Nanoscience
Vol. 17, 1–9, 2020

Majorana Field Effect Transistor. Majorana Fermion Detection and Transport Properties

Miraci S. Costa[1], Antônio T. M. Beirão[2], Carlos A. B. da Silva Jr.[3,*], Shirsley J. S. da Silva[3], and Jordan Del Nero[4]

[1] *Pós-graduação em Física, Universidade Federal do Pará, Belém-PA, 66075-110, Brazil*
[2] *Campus de Parauapebas, Universidade Federal Rural da Amazônia, Parauapebas-PA, 68515-000, Brazil*
[3] *Faculdade de Física, Universidade Federal do Pará, Ananindeua-PA, 67030-000, Brazil*
[4] *Faculdade de Física, Universidade Federal do Pará, Belém-PA, 66075-110, Brazil*

In this work we obtain analytically the transport properties as current and conductance in a toy model system formed by a quantum dot with a single level connected to a Kitaev chain deposited on a s-wave superconductor to identify the signature of Majorana zero modes (MZMs) called Majorana Fermions in solid state. For this, we use the Non-Equilibrium Green's Functions (NEGF) also named as Keldysh formalism in the matrix form to obtain the current–voltage (I–V) and conductance–voltage (G–V) curves to which goes to characterize the investigated system. Thus, it's possible to verify the presence of the Majorana Fermions in three points: (i) Conductance peak in zero polarization; (ii) The current difference depends on the asymmetry of μ_L and μ_R. We find that only for $\mu_L = \mu_R$, the source and drain currents are equal. (iii) The current difference depends on the asymmetry of Γ_L and Γ_R.

Keywords: Majorana Fermions, Kitaev Chain, Non-Equilibrium Green's Functions, Electronic Transport.

RESEARCH ARTICLE

1. INTRODUCTION

Approximately eighty years ago, Ettore Majorana proposed, in particle physics, the existence of fermions that would be his own antiparticles [1]. For several years, Majorana Fermions seemed an interesting idea, which might or might not be identified as fundamental particles in high-energy physics. Even today the neutrinos are evaluated as possible Majorana Fermions but without conclusive results.

In the last fifteen years, however, research on condensed matter has found analogues of Majorana fermions, called Majorana Zero Modes (MZMs) or Majorana Bonded States (MBSs) [2, 3], which incorporated them into the emergent form of exotic quasiparticles, exhibiting non-abelian exchange statistics [4, 5]. The search for the quasi-particles properties is beyond concern in fundamental physics, but also due to its properties of braiding that offer possible applications in quantum computing, such as a qubit with decoherence-free states under local nonuniformity [6, 7].

In the physics of condensed matter, the prototype device that can host the excitations of quasi-particles that have exactly the shape of Majorana fermions is the superconducting state. This state proved to be the viable environment of Majorana fermions the type of p-wave pairing spinless. Thus, a semiconductor-superconducting hybrid nanostructure has recently become a dominant experimental setup for the realization of Majorana superconductors and fermions [8–11]. These states have already been observed at the ends of one-dimensional (1D) superconducting wires [12–14] and in the vortex nuclei of two-dimensional (2D) topological superconductors [4–5, 8–10].

Recent works have used several shapes of superconducting nanowires coupled to quantum dots (QDs) [15–18] and calculated the transport properties as differential conductance (dI/dV). Our work seeks to advance in this field by corroborating with the calculation of transport properties such as the electric current measured at the QDs for the case of several sites in the Kitaev chain.

In this work, we propose a setup of a QDs coupled to a Kitaev chain, which is deposited on a superconducting substrate, to study the tunneling transport of Majorana

*Author to whom correspondence should be addressed.

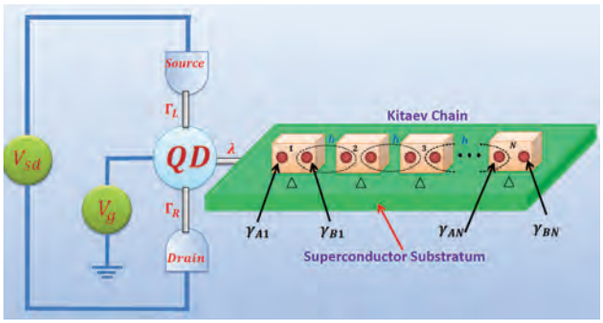

Fig. 1. System model: a single-level quantum dot coupled by two electrodes with their Γ_L and Γ_R couplings, source (emitter) and drain (receiver), and connected via constant coupling λ to a Kitaev chain with N sites, γ_{A1} and γ_{B1} are the Majorana modes of site 1, and γ_{AN} and γ_{BN} are Majorana modes at the N-site. The chain-internal coupling constants are given by h, hopping, and the Cooper parameter, Δ, representing the interaction between the sites of the chain and the substrate (topological superconductor with p-wave pairing).

fermions. The parameters of the chemical potential μ, hopping h and pairing amplitude Δ induces relatively complex couplings emphasizing that the topological phase $\mu = 0$ and $\Delta = h \neq 0$ will be investigated in the paper.

The nanowire [19] on the superconductor is then coupled to a QD which in turn is connected to two normal metal leads in order to measure the currents. For our study, we applied the non-equilibrium Green's function (NEGF) method of the Keldysh formalism to obtain the tunneling Hamiltonian current response [15–23]. In this case, the "toy" model introduced by Alexei Kitaev establishes that, for infinitely long chains (where an overlap between the final modes of Majorana is absent). In this paper, we consider the case of short chain, in the case 2-site Kitaev chain (with non-zero overlap between Majorana). Once discussed by Mourik et al. is experimentally relevant study finite-length chains.

We investigate numerically the non-equilibrium quantum transport [24, 25], calculating the electric current, continuously from the boundary of zero bias, to the regime of high polarizations, and location of the MBS effects due to asymmetric electrodes through a QD, due to the Majorana bonded states at the ends of the Kitaev chain (nanowire). The paper is organized as follows: In Section 2, we introduce our model of the T-shaped system, and your Hamiltonian. Then, we present the equations of the NEGF method and perform calculations to obtain the Green's function, current and conductance of the model proposed in the Figure 1 for a finite quantity of sites (2–6 sites). In Section 3, we present and analyze the results of our calculations of the electronic transport for 2-site Kitaev chain.

2. METHODOLOGY

We consider a single-level QD, in contact with spinless leads, coupled to a nanowire of atoms formed by Kitaev chain above a topological superconductor with p-wave pairing, illustrated in Figure 1.

The Hamiltonian of the model that describes this structure is given by:

$$\mathcal{H} = \mathcal{H}_D + \mathcal{H}_L + \mathcal{H}_{\mathrm{DE}} + \mathcal{H}_{\mathrm{DK}} + \mathcal{H}_K \tag{1}$$

The first term is the Hamiltonian of the QD, $\mathcal{H}_D = \epsilon_d d^\dagger d$, which describes the QD with a tunable level ϵ_d. Since $d^\dagger(d)$ creates (annihilates) an electron at the QD. The second term is the Hamiltonian of the electrodes (left and right) given by $\mathcal{H}_E = \sum_{k\alpha} \epsilon_k c^\dagger_{k\alpha} c_{k\alpha}$, with chemical potential μ_α. Since $c^\dagger_{k\alpha}(c_{k\alpha})$ are fermionic operators of creation (annihilation). The third term is the Hamiltonian that describes the coupling between the QD and the electrodes (tunneling Hamiltonian) given by:

$$\mathcal{H}_{DE} = \sum_{k\alpha} V_{k\alpha,n} c^\dagger_{k\alpha} d + V^*_{k\alpha,n} d^\dagger c_{k\alpha} + W_{k\alpha,n} c^\dagger_{k\alpha} d^\dagger + W^*_{k\alpha,n} dc_{k\alpha} \tag{2}$$

The Hamiltonian contains in addition to terms corresponding to the electron–electron tunneling, we have terms corresponding to the anomalous tunneling, that is, the tunneling electron–holes. Since $V_{k\alpha}$ and $W_{k\alpha,n}$ respectively represent the electron–electron and electron–hole tunneling, between the QD and the electrodes. The coupling between the QD and the first site of the chain is given by the fourth term: $\mathcal{H}_{DK} = \lambda(d^\dagger c_1 + c_1^\dagger d)$, where λ is a coupling parameter. Since $c_1^\dagger(c_1)$ are creating (annihilation) operators at the first site of the chain. The Kitaev wire is represented by:

$$\mathcal{H}_K = -\mu \sum_{j=1}^{N} c_j^\dagger c_j - \frac{1}{2} \sum_{j=1}^{N-1} \left(h c_j^\dagger c_{j+1} + h c_{j+1}^\dagger c_j + \Delta c_j c_{j+1} + \Delta^* c_{j+1}^\dagger c_j^\dagger \right) \tag{3}$$

We investigate the Majorana current from the left/right electrode to the QD. The current in the electrode α is calculated using NEGF [16]. The current is given by the charge change rate at the electrodes, and can be calculated from the definition, $I_\alpha = -(e/\hbar)\langle \dot{N}_\alpha \rangle$, where $e > 0$ is the modulus of the electric charge. $N_\alpha = \sum_k c_k^\dagger c_k$ is the total number operator for the electrode α and $\langle \cdots \rangle$ is a thermodynamic average, i.e., the mean in the ensemble relative to the Hamiltonian of the model. The derivative in the time of N_α is calculated by the Heisenberg motion equation, $\dot{N}_\alpha = (i/\hbar)[\mathcal{H}, N_\alpha]$, which results in:

$$I_\alpha = \frac{2e}{\hbar} \mathcal{R}e \left\{ \sum_{kn} V_{k\alpha,n} G^<_{n,k\alpha}(t,t) - \sum_{kn} W_{k\alpha,n} F^<_{n,k\alpha}(t,t) \right\} \tag{4}$$

being that $G^<_{n,k\alpha}(t,t) = i\langle c^\dagger_{k\alpha}(t) d(t) \rangle$ and $F^<_{n,k\alpha}(t,t) = i\langle c^\dagger_{k\alpha}(t) d^\dagger(t) \rangle$. From a direct calculation, the expression for the current can be given by:

$$I_\alpha = -\frac{e}{\hbar} \sum_{\alpha'} \int \frac{d\varepsilon}{2\pi} [\mathcal{T}^{ee}_{\alpha\alpha'}(\omega)(f_e^\alpha - f_e^{\alpha'}) - \mathcal{T}^{eh}_{\alpha\alpha}(\omega) \times (f_h^\alpha - f_e^\alpha)] \tag{5}$$

where $\mathcal{T}^{ee}_{\alpha\alpha'}(\omega) = Tr\{G^r(\omega)\Gamma^e_{\alpha'}(\omega)G^a(\varepsilon)\Gamma^e_{\alpha}(\omega)\}$, $\mathcal{T}^{eh}_{\alpha\alpha}(\omega) = Tr\{G^r(\omega)\Gamma^e_{\alpha}(\omega)G^a(\omega)\Gamma^h_{\alpha}(\omega)\}$, are the electron–electron and electron–hole transmittances, respectively. we calculate the current for the case of the QD have a single tunable level and can be modeled from Eq. (6) as follows:

$$I_\alpha = \frac{ie}{2\hbar}\int\frac{d\omega}{2\pi}\Re e\{G^r_d(\omega)[\Gamma^\alpha_e(\omega)f^\alpha_e(\omega) - \Gamma^\alpha_h(-\omega)f^\alpha_h(-\omega)] + G^<_d(\omega)[\Gamma^\alpha_e(\omega) - \Gamma^\alpha_h(-\omega)]\} \quad (6)$$

Since we define the bandwidths of electrons and holes [16], respectively by $\Gamma^\alpha_e = 2\pi V_{k\alpha}V^*_{k\alpha}\rho_\alpha$ and $\Gamma^\alpha_h = 2W_{k\alpha}W^*_{k\alpha}\rho_\alpha$, with ρ_α being the density of states (DOS) of the reservoir α. $f^\alpha_e(\omega)$ and $f^\alpha_h(-\omega)$ are the Fermi-Dirac distribution functions and the Green functions $G^r_d(\omega)$, $G^a_d(\omega)$ and $G^<_d(\omega)$ are the retarded, advanced and lesser Green's functions for the QD, respectively. These Green's functions can be obtained by analytic continuation of the Green's functions of ordered $G_d(\tau,\tau') = -i\langle \boldsymbol{T}_c d(\tau)d^\dagger(\tau')\rangle$, where $\boldsymbol{T}_c$ are orders operators along the Keldysh contour. Since the motion equation for $G_d(\tau,\tau')$ is structurally equivalent to the chronologically ordered Green's function $G_d(t,t') = -i\langle \boldsymbol{T}_c d(t)d^\dagger(t')\rangle$.

In proposed architecture we compute $G_d(t,t')$ by the motion equation technique for a 2-site Kitaev chain (at the end we present the Green's functions for 3, 4, 5, 6 and generalize to the case of n sites). Taking the derivative in time with respect to t we obtain:

$$\left(i\frac{\partial}{\partial t} - \epsilon_d\right)G^r_d(t,t') = \delta(t-t') + \sum_{k\alpha}(V_{k\alpha,n} + W_{k\alpha,n}) \times G^r_{c_{k\alpha}}(t,t') + \lambda G^r_{c_1}(t,t') \quad (7)$$

and the new Green's functions are defined as: $G^r_{k\alpha}(t,t') = -i\langle \boldsymbol{T}_c c_{k\alpha}(t)d^\dagger(t')\rangle$ and $G^r_{c_1}(t,t') = -i\langle \boldsymbol{T}_c c_1(t)d^\dagger(t')\rangle$. Calculating the derivative in time of these new Green's functions with respect to t we find:

$$\left(i\frac{\partial}{\partial t} - \epsilon_k\right)G^r_{k\alpha}(t,t') = (V_{k\alpha,n} + W_{k\alpha,n})G^r_d(t,t') \quad (8)$$

$$i\frac{\partial}{\partial t}G^r_{c_1}(t,t') = \lambda G^r_d(t,t') + hG^r_{c_2}(t,t') + \Delta G^r_{c^\dagger_2}(t,t') \quad (9)$$

Note that two new Green's functions appear in Eq. (9), and we define them as, $G^r_{c_2}(t,t') = -i\langle \boldsymbol{T}_c c_2(t)d^\dagger(t')\rangle$ and $G^r_{c^\dagger_2}(t,t') = i\langle \boldsymbol{T}_c c^\dagger_2(t)d^\dagger(t')\rangle$. Realizing the derivative with respect to t of these two Green's functions we arrive at:

$$i\frac{\partial}{\partial t}G^r_{c_2d_0}(t,t') = hG^r_{c_1}(t,t') - \Delta G^r_{c^\dagger_1}(t,t') \quad (10)$$

$$i\frac{\partial}{\partial t}G^r_{c^\dagger_2}(t,t') = -hG^r_{c^\dagger_1}(t,t') + \Delta G^r_{c_1}(t,t') \quad (11)$$

A further Green's functions appears in Eqs. (10) and (11), $G^r_{c^\dagger_1}(t,t') = -i\langle \boldsymbol{T}_c c^\dagger_1(t)d^\dagger(t')\rangle$, whose equation of motion can be easily calculated,

$$\frac{\partial}{\partial t}G^r_{c^\dagger_1}(t,t') = -\lambda G^r_{d^\dagger}(t,t') - hG^r_{c^\dagger_2}(t,t') - \Delta G^r_{c_2}(t,t') \quad (12)$$

It appears in Eq. (12) another Green's functions, $G^r_{d^\dagger}(t,t') = -i\langle \boldsymbol{T}_c d^\dagger_0(t)d^\dagger(t')\rangle$, calculated in:

$$\left(i\frac{\partial}{\partial t} + \epsilon_d\right)G^r_{d^\dagger}(t,t') = -\sum_{k\alpha}(V^*_{k\alpha,n} + W^*_{k\alpha,n})G^r_{c^\dagger_{k\alpha}}(t,t') - \lambda G^r_{c^\dagger_1}(t,t') \quad (13)$$

Finally, there remains a Green function given by: $G^r_{c^\dagger_{k\alpha}}(t,t') = -i\langle \boldsymbol{T}_c c^\dagger_{k\alpha}(t)d^\dagger(t')\rangle$, which results in :

$$\left(i\frac{\partial}{\partial t} + \epsilon_k\right)G^r_{c^\dagger_{k\alpha}}(t,t') = -(V^*_{k\alpha,n} + W^*_{k\alpha,n})G^r_{d^\dagger}(t,t') \quad (14)$$

The Eqs. (7)–(14) constitute a complete set of eight differential equations. In order to reduce to only six equations, we write Eqs. (8) and (14) in their integral forms:

$$G^r_{c_{k\alpha}}(t,t') = (V_{k\alpha,n} + W_{k\alpha,n})\int dt_1 g_{k\alpha}(t,t_1)G_d(t_1,t') \quad (15)$$

$$G^r_{c^\dagger_{k\alpha}}(t,t') = -(V^*_{k\alpha,n} + W^*_{k\alpha,n})\int dt_1 g'_{k\alpha}(t,t_1)G_{d^\dagger}(t_1,t') \quad (16)$$

and replacing Eqs. (15) and (16), respectively, in Eqs. (7) and (13). This gives:

$$\left(i\frac{\partial}{\partial t} - \epsilon_d\right)G^r_{d_0}(t,t') = \delta(t-t') + \int dt_1\sum(t,t_1)G^r_d(t,t') + \lambda G^r_{c_1}(t,t') \quad (17)$$

$$\left(i\frac{\partial}{\partial t} + \epsilon_d\right)G^r_{d^\dagger_0}(t,t') = -\int dt_1\sum{}'(t,t_1)G^r_{d^\dagger}(t,t') - \lambda G^r_{c^\dagger_1}(t,t') \quad (18)$$

Since we define the self-energy functions of the electrodes as:

$$\sum(t,t_1) = \sum_{k\alpha}[V_{k\alpha,n}g_{k\alpha}(t,t_1)V^*_{k\alpha,n} + W_{k\alpha,n}g_{k\alpha}(t,t_1)W^*_{k\alpha,n}] \quad (19)$$

$$\sum{}'(t,t_1) = \sum_{k\alpha}[V_{k\alpha,n}\bar{g}_{k\alpha}(t,t_1)V^*_{k\alpha,n} + W_{k\alpha,n}\bar{g}_{k\alpha}(t,t_1)W^*_{k\alpha,n}] \quad (20)$$

The Eqs. (10)–(13) and (17)–(18) constitute our new set of six integral-differential equations, which can be written in compact matrix form as:

$$\vec{G}(t,t') = g(t,t')\vec{\boldsymbol{u}} + \int\int dt_2dt_1 g(t,t_2)\sum{}''(t_2,t_1)\boldsymbol{G}(t_1,t') \quad (21)$$

RESEARCH ARTICLE

where the matrix $g(t,t')$ is given by:

$$\begin{pmatrix} i\frac{\partial}{\partial t}-\epsilon_d & 0 & 0 & 0 & 0 & 0 \\ 0 & i\frac{\partial}{\partial t}+\epsilon_d & 0 & 0 & 0 & 0 \\ 0 & 0 & i\frac{\partial}{\partial t}+\epsilon_1 & 0 & 0 & 0 \\ 0 & 0 & 0 & i\frac{\partial}{\partial t}+\epsilon_1 & 0 & 0 \\ 0 & 0 & 0 & 0 & i\frac{\partial}{\partial t}+\epsilon_2 & 0 \\ 0 & 0 & 0 & 0 & 0 & i\frac{\partial}{\partial t}+\epsilon_2 \end{pmatrix} \times g(t,t')=\delta(t-t')\mathbf{I} \quad (22)$$

with $\mathbf{I}$ being the matrix is a 6×6 identity matrix, and:

$$\tilde{\Sigma}(t_2,t_1)=\begin{pmatrix} \Sigma & 0 & 0 & 0 & 0 & 0 \\ 0 & \Sigma' & 0 & 0 & 0 & 0 \\ 0 & 0 & 0 & 0 & 0 & 0 \\ 0 & 0 & 0 & 0 & 0 & 0 \\ 0 & 0 & 0 & 0 & 0 & 0 \\ 0 & 0 & 0 & 0 & 0 & 0 \end{pmatrix}+\delta(t_1-t_2) \times \begin{pmatrix} 0 & 0 & +\lambda & 0 & 0 & 0 \\ 0 & 0 & 0 & -\lambda & 0 & 0 \\ +\lambda & 0 & 0 & 0 & +h & +\Delta \\ 0 & +\lambda & 0 & 0 & -\Delta & -h \\ 0 & 0 & +h & -\Delta & 0 & 0 \\ 0 & 0 & +\Delta & -h & 0 & 0 \end{pmatrix} \quad (23)$$

The self-energy matrix retarded:

$$\Sigma^r(\omega)=\begin{pmatrix} \Sigma & 0 & +\lambda & 0 & 0 & 0 \\ 0 & \Sigma' & 0 & -\lambda & 0 & 0 \\ +\lambda & 0 & 0 & 0 & +h & +\Delta \\ 0 & +\lambda & 0 & 0 & -\Delta & -h \\ 0 & 0 & +h & -\Delta & 0 & 0 \\ 0 & 0 & +\Delta & -h & 0 & 0 \end{pmatrix} \quad (24)$$

The vectors $\vec{G}(t,t')$ and $\vec{u}$ are defined as:

$$\vec{G}(t,t')=\begin{pmatrix} G^r_d(t,t') \\ G^r_{d^\dagger}(t,t') \\ G^r_{c_1}(t,t') \\ G^r_{c_1^\dagger}(t,t') \\ G^r_{c_2}(t,t') \\ G^r_{c_2^\dagger}(t,t') \end{pmatrix}; \quad \vec{u}=\begin{pmatrix} 1 \\ 0 \\ 0 \\ 0 \\ 0 \\ 0 \end{pmatrix} \quad (25)$$

Iterating Eq. (21), we can show that:

$$\vec{G}(t,t')=\boldsymbol{G}(t,t')\vec{u} \quad (26)$$

And we have the Dyson equation:

$$\boldsymbol{G}(t,t')=\boldsymbol{g}(t,t')+\int\int dt_2 dt_1 \boldsymbol{g}(t,t_1)\tilde{\Sigma}(t_1,t_2)\boldsymbol{G}(t_2,t') \quad (27)$$

Writing a similar equation in the Keldysh contour [26–28],

$$\boldsymbol{G}(\tau,\tau')=\boldsymbol{g}(\tau,\tau')+\int\int d\tau_2 d\tau_1 \boldsymbol{g}(\tau,\tau_1)\tilde{\Sigma}(\tau_1,\tau_2)\boldsymbol{G}(\tau_2,\tau') \quad (28)$$

applying the rules of Langreth's analytical continuation, we have for the retarded Green's function, already in the energy domain:

$$\boldsymbol{G}^r(\omega)=\boldsymbol{g}^r(\omega)+\boldsymbol{g}^r(\omega)\tilde{\Sigma}^r(\omega)\boldsymbol{G}^r(\omega) \quad (29)$$

and for the lesser Green's function:

$$\boldsymbol{G}^<(\omega)=\boldsymbol{G}^r(\omega)\tilde{\Sigma}^<(\omega)\boldsymbol{G}^a(\omega) \quad (30)$$

The components of retarded and lesser auto-energy can be expressed as:

$$\Sigma^r(\omega)=\begin{pmatrix} \Sigma & 0 & +\lambda & 0 & 0 & 0 \\ 0 & \Sigma' & 0 & -\lambda & 0 & 0 \\ +\lambda & 0 & 0 & 0 & +h & +\Delta \\ 0 & +\lambda & 0 & 0 & -\Delta & -h \\ 0 & 0 & +h & -\Delta & 0 & 0 \\ 0 & 0 & +\Delta & -h & 0 & 0 \end{pmatrix} \quad (31)$$

And the matrix $\tilde{\Sigma}^<(\omega)$ has only two nonzero elements:

$$\tilde{\Sigma}^<_{11}(\omega) = i[\Gamma_L(\omega)f_L(\omega)+\Gamma_R(\omega)f_R(\omega)+\Gamma_L(-\omega)f_L(-\omega) +\Gamma_R(-\omega)f_R(-\omega)] \quad (32)$$

$$\tilde{\Sigma}^<_{22}(\omega) = i[\Gamma_L(-\omega)f_L(-\omega)+\Gamma_R(-\omega)f_R(-\omega) +\Gamma_L(\omega)f_L(\omega)+\Gamma_R(\omega)f_R(\omega)] \quad (33)$$

With the other elements of $\tilde{\Sigma}^<(\omega)$ equal to zero. To obtain $G^r_d(\omega)$ and $G^a_d(\omega)$ we must find $\boldsymbol{G}^r(\omega)$ in Eq. (29). We get, after using matrices properties:

$$\{\boldsymbol{G}^r(\omega)\}^{-1}=[\boldsymbol{g}^r(\omega)]^{-1}-\tilde{\Sigma}^r(\omega) \quad (34)$$

Therefore:

$$\{\boldsymbol{G}^r(\omega)\}^{-1}=\begin{pmatrix} G_0 & 0 & -\lambda & 0 & 0 & 0 \\ 0 & G_{\overline{0}} & 0 & +\lambda & 0 & 0 \\ -\lambda & 0 & G_1 & 0 & -h & -\Delta \\ 0 & +\lambda & 0 & G_1 & +\Delta & +h \\ 0 & 0 & -h & +\Delta & G_2 & 0 \\ 0 & 0 & -\Delta & +h & 0 & G_2 \end{pmatrix} \quad (35)$$

RESEARCH ARTICLE

In order to facilitate the generalization to n sites, we will consider Eq. (35) in the form of a block matrix:

$$\{\boldsymbol{G}^r(\omega)\}^{-1}=\begin{pmatrix}\boldsymbol{G_0} & \Lambda & \boldsymbol{0}\\ \Lambda & \boldsymbol{G_1} & \boldsymbol{A}\\ \boldsymbol{0} & \boldsymbol{B} & \boldsymbol{G_2}\end{pmatrix} \tag{36}$$

Where the submatrices are given by:

$$\boldsymbol{G_0}=\begin{pmatrix}G_0 & 0\\ 0 & G_{\overline{0}}\end{pmatrix};\quad \Lambda=\begin{pmatrix}-\lambda & 0\\ 0 & +\lambda\end{pmatrix};\quad \mathbf{A}=\begin{pmatrix}-h & -\Delta\\ +\Delta & +h\end{pmatrix};$$

$$\mathbf{B}=\begin{pmatrix}-h & +\Delta\\ -\Delta & +h\end{pmatrix};\quad \boldsymbol{0}=\begin{pmatrix}0\,0\\ 0\,0\end{pmatrix};\quad \boldsymbol{G_1}=\begin{pmatrix}G_1 & 0\\ 0 & G_1\end{pmatrix};$$

$$\boldsymbol{G_2}=\begin{pmatrix}G_2 & 0\\ 0 & G_2\end{pmatrix}.$$

Thus, the matrix of the Green's function of the system for 3 sites will be given by:

$$\{\boldsymbol{G}^r(\omega)\}^{-1}=\begin{pmatrix}\boldsymbol{G_0} & \Lambda & \boldsymbol{0} & \boldsymbol{0}\\ \Lambda & \boldsymbol{G_1} & \boldsymbol{A} & \boldsymbol{0}\\ \boldsymbol{0} & \boldsymbol{B} & \boldsymbol{G_2} & \boldsymbol{A}\\ \boldsymbol{0} & \boldsymbol{0} & \boldsymbol{B} & \boldsymbol{G_3}\end{pmatrix} \tag{37}$$

com

$$\boldsymbol{G_3}=\begin{pmatrix}G_3 & 0\\ 0 & G_3\end{pmatrix}$$

And for 4, 5 and 6 sites, respectively, we have:

$$\{\boldsymbol{G}^r(\omega)\}^{-1}=\begin{pmatrix}\boldsymbol{G_0} & \Lambda & \boldsymbol{0} & \boldsymbol{0} & \boldsymbol{0}\\ \Lambda & \boldsymbol{G_1} & \boldsymbol{A} & \boldsymbol{0} & \boldsymbol{0}\\ \boldsymbol{0} & \boldsymbol{B} & \boldsymbol{G_2} & \boldsymbol{A} & \boldsymbol{0}\\ \boldsymbol{0} & \boldsymbol{0} & \boldsymbol{B} & \boldsymbol{G_3} & \boldsymbol{A}\\ \boldsymbol{0} & \boldsymbol{0} & \boldsymbol{0} & \boldsymbol{B} & \boldsymbol{G_4}\end{pmatrix} \tag{38}$$

$$\{\boldsymbol{G}^r(\omega)\}^{-1}=\begin{pmatrix}\boldsymbol{G_0} & \Lambda & \boldsymbol{0} & \boldsymbol{0} & \boldsymbol{0} & \boldsymbol{0}\\ \Lambda & \boldsymbol{G_1} & \boldsymbol{A} & \boldsymbol{0} & \boldsymbol{0} & \boldsymbol{0}\\ \boldsymbol{0} & \boldsymbol{B} & \boldsymbol{G_2} & \boldsymbol{B} & \boldsymbol{0} & \boldsymbol{0}\\ \boldsymbol{0} & \boldsymbol{0} & \boldsymbol{A} & \boldsymbol{G_3} & \boldsymbol{A} & \boldsymbol{0}\\ \boldsymbol{0} & \boldsymbol{0} & \boldsymbol{0} & \boldsymbol{B} & \boldsymbol{G_4} & \boldsymbol{A}\\ \boldsymbol{0} & \boldsymbol{0} & \boldsymbol{0} & \boldsymbol{0} & \boldsymbol{B} & \boldsymbol{G_5}\end{pmatrix} \tag{39}$$

$$\{\boldsymbol{G}^r(\omega)\}^{-1}=\begin{pmatrix}\boldsymbol{G_0} & \Lambda & \boldsymbol{0} & \boldsymbol{0} & \boldsymbol{0} & \boldsymbol{0} & \boldsymbol{0}\\ \Lambda & \boldsymbol{G_1} & \boldsymbol{A} & \boldsymbol{0} & \boldsymbol{0} & \boldsymbol{0} & \boldsymbol{0}\\ \boldsymbol{0} & \boldsymbol{B} & \boldsymbol{G_2} & \boldsymbol{A} & \boldsymbol{0} & \boldsymbol{0} & \boldsymbol{0}\\ \boldsymbol{0} & \boldsymbol{0} & \boldsymbol{B} & \boldsymbol{G_3} & \boldsymbol{A} & \boldsymbol{0} & \boldsymbol{0}\\ \boldsymbol{0} & \boldsymbol{0} & \boldsymbol{0} & \boldsymbol{B} & \boldsymbol{G_4} & \boldsymbol{A} & \boldsymbol{0}\\ \boldsymbol{0} & \boldsymbol{0} & \boldsymbol{0} & \boldsymbol{0} & \boldsymbol{B} & \boldsymbol{G_5} & \boldsymbol{A}\\ \boldsymbol{0} & \boldsymbol{0} & \boldsymbol{0} & \boldsymbol{0} & \boldsymbol{0} & \boldsymbol{B} & \boldsymbol{G_6}\end{pmatrix} \tag{40}$$

And, therefore, generalizing for n sites, we have:

$$\{\boldsymbol{G}^r(\omega)\}^{-1}=\begin{pmatrix}\boldsymbol{G_0} & \Lambda & \boldsymbol{0} & \boldsymbol{0} & \boldsymbol{0} & & \boldsymbol{0} & \boldsymbol{0} & \boldsymbol{0} & \boldsymbol{0} & \boldsymbol{0}\\ \Lambda & \boldsymbol{G_1} & \boldsymbol{0} & \boldsymbol{0} & \boldsymbol{0} & & \boldsymbol{\lambda} & \boldsymbol{0} & \boldsymbol{0} & \boldsymbol{0} & \boldsymbol{0}\\ \boldsymbol{0} & \boldsymbol{B} & \boldsymbol{G_2} & \boldsymbol{A} & \boldsymbol{0} & \cdots & \boldsymbol{0} & \boldsymbol{0} & \boldsymbol{0} & \boldsymbol{0} & \boldsymbol{0}\\ \boldsymbol{0} & \boldsymbol{0} & \boldsymbol{B} & \boldsymbol{G_3} & \boldsymbol{A} & & \boldsymbol{0} & \boldsymbol{0} & \boldsymbol{0} & \boldsymbol{0} & \boldsymbol{0}\\ \boldsymbol{0} & \boldsymbol{0} & \boldsymbol{0} & \boldsymbol{B} & \boldsymbol{G_4} & & \boldsymbol{0} & \boldsymbol{0} & \boldsymbol{0} & \boldsymbol{0} & \boldsymbol{0}\\ & & \vdots & & & \ddots & & \vdots & & & \\ \boldsymbol{0} & \boldsymbol{0} & \boldsymbol{0} & \boldsymbol{0} & \boldsymbol{0} & & \boldsymbol{G_{n-4}} & \boldsymbol{A} & \boldsymbol{0} & \boldsymbol{0} & \boldsymbol{0}\\ \boldsymbol{0} & \boldsymbol{0} & \boldsymbol{0} & \boldsymbol{0} & \boldsymbol{0} & & \boldsymbol{B} & \boldsymbol{G_{n-3}} & \boldsymbol{A} & \boldsymbol{0} & \boldsymbol{0}\\ \boldsymbol{0} & \boldsymbol{0} & \boldsymbol{0} & \boldsymbol{0} & \boldsymbol{0} & \cdots & \boldsymbol{0} & \boldsymbol{B} & \boldsymbol{G_{n-2}} & \boldsymbol{A} & \boldsymbol{0}\\ \boldsymbol{0} & \boldsymbol{0} & \boldsymbol{0} & \boldsymbol{0} & \boldsymbol{0} & & \boldsymbol{0} & \boldsymbol{0} & \boldsymbol{B} & \boldsymbol{G_{n-1}} & \boldsymbol{A}\\ \boldsymbol{0} & \boldsymbol{0} & \boldsymbol{0} & \boldsymbol{0} & \boldsymbol{0} & & \boldsymbol{0} & \boldsymbol{0} & \boldsymbol{0} & \boldsymbol{B} & \boldsymbol{G_n}\end{pmatrix} \tag{41}$$

Where:

$$\boldsymbol{G_n}=\begin{pmatrix}G_n & 0\\ 0 & G_n\end{pmatrix}$$

Using the Eqs. (25) and (26) in the frequency domain, we obtain:

$$\vec{G}(\omega)=\boldsymbol{G}^r(\omega)\vec{\boldsymbol{u}}$$

Or yet, in the case of 2 sites in the Kitaev chain:

$$\begin{pmatrix}G^r_d(\omega)\\ G^r_{d^\dagger}(\omega)\\ G^r_{c_1}(\omega)\\ G^r_{c_1^\dagger}(\omega)\\ G^r_{c_2}(\omega)\\ G^r_{c_2^\dagger}(\omega)\end{pmatrix}=\boldsymbol{G}(\omega)\begin{pmatrix}1\\ 0\\ 0\\ 0\\ 0\\ 0\end{pmatrix} \tag{42}$$

And using the property, we have the advanced Green's function:

$$G^a_d(\omega)=[G^r_d(\omega)]^* \tag{43}$$

We will get the advanced Green function of the quantum dot. With these equations we can calculate the transport properties described below.

3. NUMERICAL RESULTS

According to the Keldysh formalism developed in the previous section, we performed the numerical calculation to investigate the transport properties of electrons and holes in the T-shaped system of QD and a 1D topological superconductor with Majorana fermions at the ends of a Kitaev chain with 2 sites. We consider the most studied and completely soluble case for the Kitaev chain, $\mu=0$ and

RESEARCH ARTICLE

$\Delta = t \neq 0$. We can verify the presence of the fermions of Majorana from three points: (i) Conductance peak in zero polarization; (ii) The current difference depends on the asymmetry of μ_L and μ_R. In particular, we find that only for $\mu_L = \mu_R$, the source and drain currents are equals. (iii) The current difference depends on the asymmetry of Γ_L and Γ_R. In particular, we find that (only) for $\Gamma_L = \Gamma_R$ the source and drain currents are equal to each other.

MBS Signature-In the following numerical calculations, we investigate the single-level case $\epsilon_d = 0$. In Figure 2(a), we have the case of $\lambda = 0$(coupled dot−chain), that is, the Kitaev chain is decoupled. We have only the QD coupled to the electrodes. The differential conductance (dI/dV) curve exhibits a peak at the zero-bias point, typical sign of common fermions (electrons). In Figure 2(b), we incorporate the coupling between QD and $\gamma_{A,1}$, in this case, of $\lambda \neq 0$. However, we have not yet connected the superconducting substrate, i.e., $\Delta = h = 0$. The conductance exhibits two peaks at the points of $V_b = \pm 2,3$ V at the point $V_b = 0$ becomes zero.

In Figure 2(c), we display $\lambda \neq 0$ and $\Delta = h \neq 0$. The conductance still exhibits two peaks at the points of $V_b = \pm 2,3$ V, but at the point $V_b = 0$ shows a peak which is of the same intensity as the half of the electron-relative peak. Then, when the coupling between QD and $\gamma_{A,1}$ is incorporated, we can clearly see that the conductance peak. The interesting thing is that, in the presence of non-zero λ, the conductance at the point of zero polarization shows a peak. By further observation, we know that the conductance value at the zero point of the energy is exactly equal to $e^2/2h$. With the increase of such coupling, this conductance peak is enlarged, leaving its peak height unchanged. A zero-bias DC current conductance peak appears in our configuration, which means the existence of Majorana fermion and is in accordance with previous experimental results on the InSb nanowire. Recent experimental and theoretical investigations for signal signatures similar to Majorana modes (Andreev zero modes and Kondo resonance) in semiconductor nanowires with proximity effect involve conductance spectroscopy, where the evidence sought is a robust zero polarization peak, which determines the convincing signature of MZMs [29, 30]. As a result, in general the characteristic I–V curve show in the linear response regime (bias$\rightarrow$0 V) a finite slope as the bias increases. The dI/dV curve shows the presence of three peak with one Majorana mode pinned at 0.5 V for 0 V.

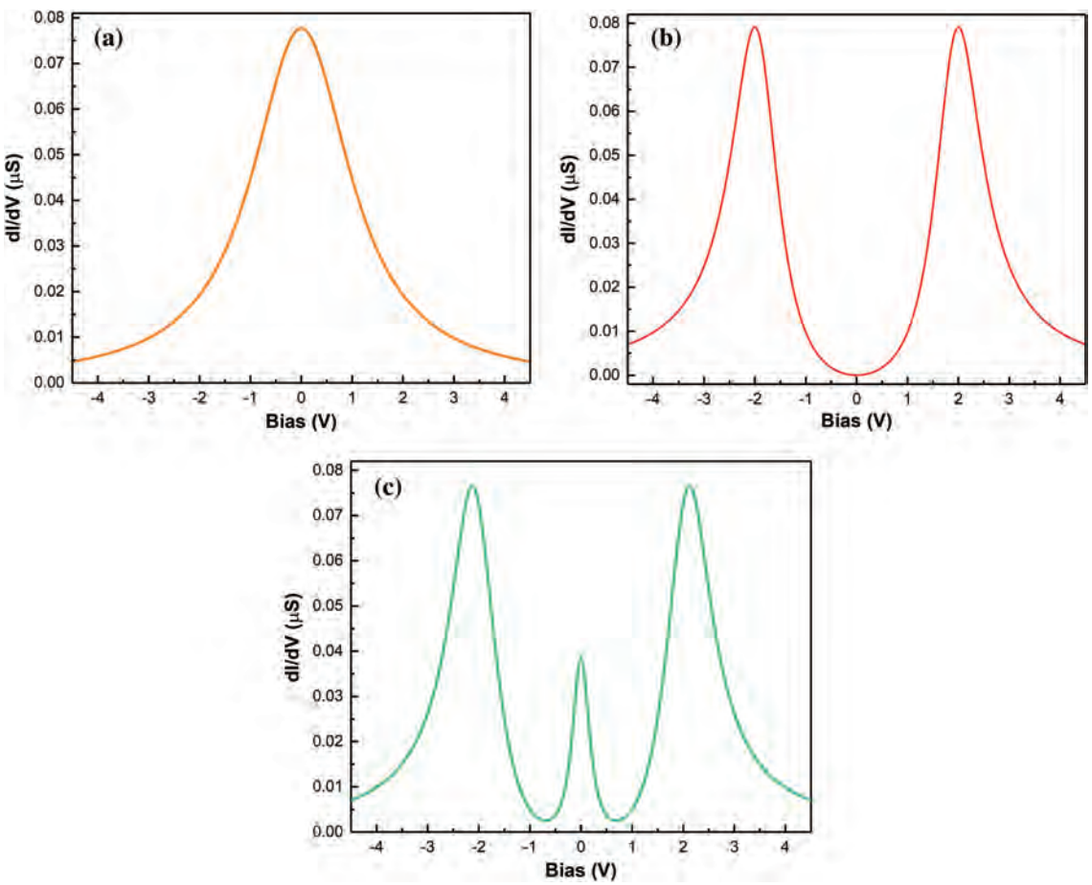

Fig. 2. dI/dV curves for $\lambda = 0$ the behaves as (a) single-level QD, (b) flat for the regular fermion situation and (c) In the presence of a MBS.

RESEARCH ARTICLE

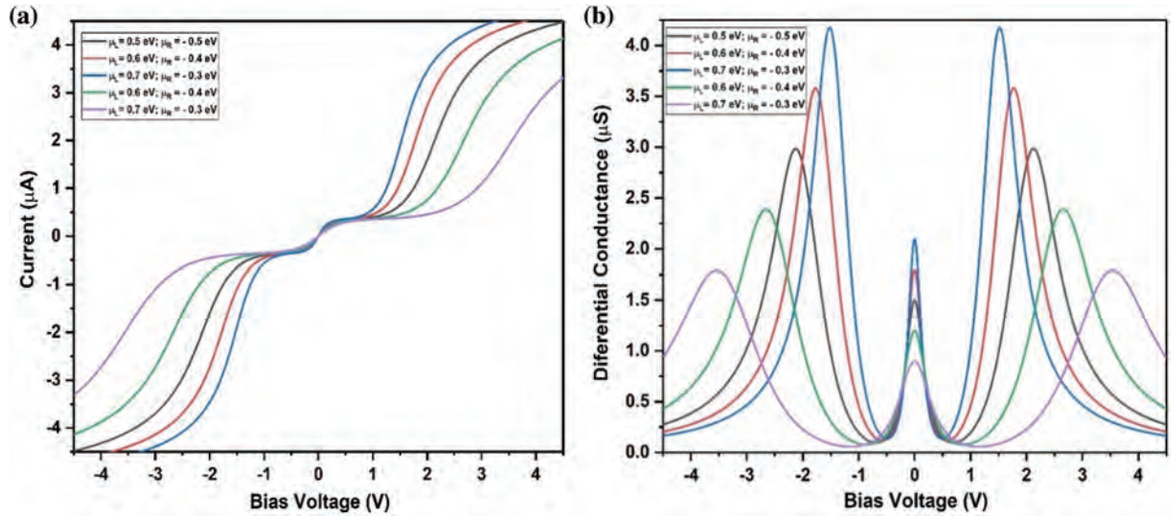

Fig. 3. (a) I–V curve (b) dI/dV–V curve as function of bias voltage for several chemical potential μ. For left electrode, $\mu_L = 0.5$, $\mu_L = 0.5$ (black line); $\mu_L = 0.6$, $\mu_L = 0.4$ (red line); $\mu_L = 0.7$, $\mu_L = 0.3$ (blue line) and for right electrode $\mu_R = 0.5$ (black line); $\mu_R = 0.6$, $\mu_R = 0.4$ (green line); $\mu_R = 0.7$, $\mu_R = 0.3$ (lilac line).

We then investigate the response of the system under study for the characteristics I–V and dI/dV–V curves applied at the two electrodes of the QD, defining the polarization in these by $V = (\mu_L - \mu_R)/e$. Varying the chemical potentials of the right and left electrodes. The results show the emergence of the Majorana modes with the presence of the superconducting substrate a new load carrier channel appears, in the case of holes. Therefore we have the transport of electrons and holes carriers, Majorana transport. This result certainly leads to a variation in the transport of ordinary electron tunneling [16]. In this case, in general, when we vary the values of the chemical potentials, we verify the non-conservation of the current of the electrodes, i.e., $I_L \neq -I_R$. When the hole transmission factor, $M_{eh}^{\alpha\alpha}$ vanish, the conservation of the current is recovered, $I_L = -I_R$, i.e., when $\mu_L = \mu_R$.

Therefore, the non-conservation of current is a unique characteristic that marks the Majorana transport. So, we have another way that characterizes a Majorana mode. In general, we can define the Majorana current as $(I_L - I_R)/2$. When we turn off the superconductor we recover the ordinary case.

We have argued that it is necessary to investigate the case of the asymmetrical coupling of quantum electrodes. We found that when $\Gamma^L \neq \Gamma^R$, the currents on the two

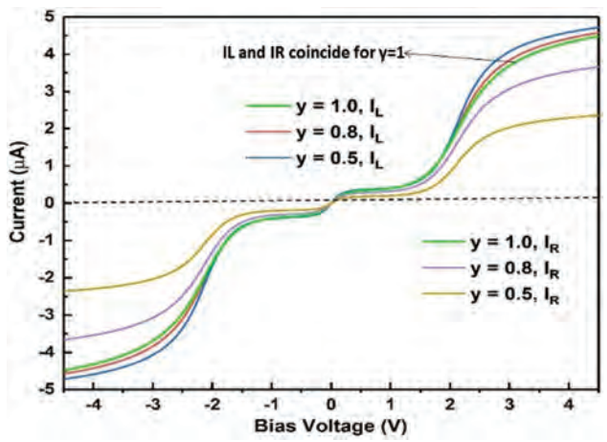

Fig. 4. (Color online) Left lead current (I_L) and right lead current (I_R) against the bias voltage. For $\lambda \neq 0$ (MBS), for two asymmetry factors $y = 0.5$ and $y = 0.8$ and symmetric factor $y = 1$ (green line). The current–voltage curve is not conserve (IL ≠ IR). For voltages V > 2.0, currents IL and IR reach different plateaus. In this case, we have the current $|IL| > |GO|$ for asymmetry of electrodes $y = 0.5$ and $|IL| > |GO|$ for asymmetry of the electrodes $y = 0.8$.

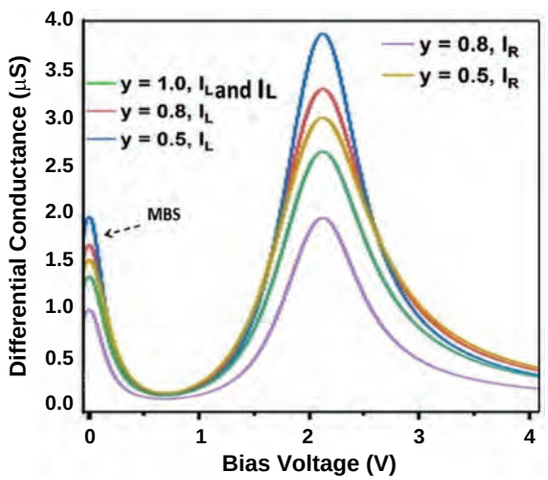

Fig. 5. (Color online) Differential conductance dI/dV for left lead Γ^L and right lead Γ^R against the bias voltage. For $\lambda \neq 0$ (MBS), for two asymmetry factors $y = 0.5$ and $y = 0.8$ and symmetric factor $y = 1$ (green line). The differential conductance dI_L/dV and dI_R/dV clearly show the symmetric case, where both conductance are at 0.5.

RESEARCH ARTICLE

normal electrodes are different, because of Andreev's reflections due to the two MBS. Here we define an asymmetry coefficient $y=\Gamma^R/\Gamma^L$. In Figures 4 and 5, we vary the parameter y and determine the I–V and dI/dV–V curves. We find that, in the absence of MBS, the magnitudes of the I–V curve are equals in both electrodes, i.e., when $y=1$, $(\Gamma^L=\Gamma^R)$, the asymmetry becomes accentuated when we decrease y, when the MBS is introduced, the current results on the two electrodes become different from each other.

To decrease and weaken Andreev's reflection on the R electrode, but strengthens this in the electrode L, leading to different currents and conductance in the two terminals. Despite the difference in current and conductance, the presence of MBS-induced conductance peak can still be observed in the case of the asymmetric coupling quantum-point electrodes. So far, we know that in this structure, the detection of MBS is independent of the way of coupling quantum dot-electrodes.

4. CONCLUSION

In this paper, we use the formalism of Keldysh to calculate the functions of Green [31] smaller and larger Green of the chain of Kitaev for the calculation of the current. A zero bias current conductance peak appears in our differential conductance graphs, which implies the existence of the Majorana fermion and is consistent with previous experiments on the nanowire [12, 13]. We find that, like the fermion of Majorana that is its own antiparticle, there is a channel of transmission of holes that makes the currents of the electrodes not conserved. This non-conservation of the current can be used as a criterion for detecting Majorana fermion. Our results are consistent with previous studies in the literature that calculate electronic transport using the theory of nonlinear response. Our I–V curves show a characteristic slope given by $I=(G_0/2)V$, with half the ballistic conductance $G_0=e^2/h$, as predicted [29–30]. We also calculate the differential conductance obtained from the right and left currents. The coupled in Figure 1 parameters, are based in the type of geometry studied for to allow realise more realistic experiment in the case: (i) an optical grid, feasible through use of the cold atoms technique and (ii) partnered with another technique, such as Mechanical Break Junction (MBJ) [32–33] due to the dot-chain interface in the T-shaped geometry [34].

Acknowledgments: The authors thank the Brazilian funding agencies CNPq, CAPES, PROPESP (EDITAL PAPQ 01/2020) and Campus Ananindeua-UFPA.

References

1. Majorana, E., **1937**. Teoria simmetrica dell'eletrone e dell positrone. II. *Nuovo Cimento, 14*(4), pp.171–184.
2. Stern, A., **2010**. Non-abelian states of matter. *Nature, 464*(7286), pp.187–193.
3. Nayak, C., Simon, S.H., Stern, A., Freedman, M. and Das Sarma, S., **2008**. Non-abelian anyons and topological quantum computation. *Reviews of Modern Physics, 80*(3), pp.1083–1159.
4. Kitaev, A.Y., **2001**. Unpaired majorana fermions in quantum wires. *Physics-Uspekhi, 44*(10S), pp.131–136.
5. Kitaev, A.Y., **2003**. Fault-tolerant quantum computation by anyons. *Annals of Physics, 303*(1), pp.2–30.
6. Moore, G. and Read, N., **1991**. Nonabelian in the fractional quantum hall effect. *Nuclear Physics B, 360*(2–3), pp.362–396.
7. Fu, L. and Kane, C.L., **2008**. Superconducting proximity effect and majorana fermions at the surface of a topological insulator. *Physical Review Letters, 100*(9), pp.0964071–0964074.
8. Oreg, Y., Refael, G. and von Oppen, F., **2010**. Helical liquids and majorana bound states in quantum wires. *Physical Review Letters, 105*(17), pp.1–4.
9. Mourik, V., Zuo, K., Frolov, S.M., Plissard, S.R., Bakkers, E.P.A.M. and Kouwenhoven, L.P., **2012**. Signatures of majorana fermions in hybrid superconductor-semiconductor nanowire devices. *Science, 336*(6084), pp.1003–1007.
10. Nadj-Perge, S., Drozdov, I.K., Li, J., Chen, H., Jeon, S., Seo, J., MacDonald, A.H., Bernevig, B.A. and Yazdani, A., **2014**. Observation of majorana fermions in ferromagnetic atomic chains on a superconductor. *Science, 346*(6209), pp.602–607.
11. Alicea, J., **2010**. Majorana fermions in a tunable semiconductor device. *Physical Review B, 81*(12), pp.1–10.
12. Sau, J.D., Lutchyn, R.M., Tewari, S. and Das Sarma, S., **2010**. Generic new platform for topological quantum computation using semiconductor heterostructures. *Physical Review Letters, 104*(4), pp.1–4.
13. Jünger, C., Baumgartner, A., Delagrange, R., Raphaelle, D., Chevallier, D., Lehmann, S., Dick, A.K., Thelander, C. and Schönenberger, C., **2019**. Spectroscopy of the superconducting proximity effect in nanowires using integrated quantum dots. *Communications Physics, 2*(76), pp.1–8.
14. Chen, Q. and Xu, N., **2018**. Shot noise in superconducting wires applied with a periodic electric field. *Journal of Nanoscience and Nanotechnology, 18*(5), pp.3729–3733.
15. Liu, D.E. and Baranger, H.U., **2011**. Detecting a majorana-fermion zero mode using a quantum dot. *Physical Review B, 84*(20), pp.1–4.
16. Gong, W.-J., Zhang, S.-F., Li, Z.-C., Yi, G. and Zheng, Y.-S., **2014**. Detection of a majorana fermion zero mode by a T-shaped quantum-dot structure. *Physical Review B, 89*(24), pp.1–8.
17. Cao, Y., Wang, P., Xiong, G., Gong, M. and Li, X.-Q., **2012**. Probing the existence and dynamics of Majorana fermion via transport through a quantum dot. *Physical Review B, 86*(11), pp.1–5.
18. You, J.-B., Shao, X.-Q., Tong, Q.-J., Chan, A.H., Oh, C.H. and Vedral, V., **2015**. Majorana transport in superconducting nanowire with Rashba and Dresselhaus spin–orbit couplings. *Journal of Physics: Condensed Matter, 27*(22), pp.1–14.
19. Petrychuk, M., Zadorozhnyi, I., Kutovyi, Y., Karg, S., Riel, H. and Vitusevich, S., **2019**. Noise spectroscopy to study the 1D electron transport properties in InAs nanowires. *Nanotechnology, 30*(1), pp.1–9.
20. Lishu, Z., Xinyue, D., Yi, Z., Zhenyang, Z., Longwei, Y. and Hui, L., **2017**. Theoretical study of electronic transport properties of lead nanowires doped with silicon. *Computational Materials Science, 136*(1), pp.198–206.
21. Karen, M., David, N., David, H.W. and Ron, N., **2019**. Voltage-induced long-range coherent electron transfer through organic molecules. *Proceedings of the National Academy of Sciences, 116*(13), pp.5931–5936.
22. Saeideh, M., Davoud, P., Reinhard, S. and Thomas, G., **2008**. Electronic transport properties in copper nanowire. *Microelectronic Engineering, 85*(10), pp.1992–1994.
23. Thingna, J., Manzano, D. and Cao, J., **2016**. Dynamical signatures of molecular symmetries in nonequilibrium quantum transport. *Scientific Reports, 6*(28027), pp.1–11.

24. Zheng, Y.D., **2019**. Analysis of nonequilibrium transport properties of interacting quantum wire model. *Journal of Applied Mathematics and Physics, 7*(8), pp.1677–1685.
25. Meir, Y. and Wingreen, N.S., **1992**. Landauer formula for the current through an interacting electron region. *Physical Review Letters, 68*(16), pp.2512–2515.
26. Jauho, A.P., Wingreen, N.S. and Meir, Y., **1994**. Time-dependent transport in interacting and noninteracting resonant-tunneling systems. *Physical Review B, 50*(8), pp.5528–5547.
27. Datta, S., **2005**. Quantum transport: Atom to transistor. Cambridge University Press.
28. Flensberg, K., **2010**. Tunneling characteristics of a chain of Majorana bound states. *Physical Review B, 82*(18), pp.1–4.
29. Beirão, A.T.M., Costa, M.S., de Oliveira, A.S., Da, C., Cunha, J.J., da Silva, S.S. and Del Nero, J., **2018**. Majorana bound states in a quantum dot device coupled with a superconductor zigzag chain. *Journal of Computational Electronics, 17*(3), pp.959–966.
30. Langreth, D.C. and Nordlander, P., **1991**. Derivation of a master equation for charge-transfer processes in atom-surface collisions. *Physical Review B, 43*(4), pp.2541–2557.
31. Caussanel, M., Schrimpf, R.D., Tsetseris, L., Evans, M.H. and Pantelides, S.T., **2007**. Engineering model of a biased metal–molecule–metal junction. *Journal of Computational Electronics, 6*(4), pp.425–430.
32. Sabater, C., Untiedt, C. and Van Ruitenbeek, J.M., **2015**. Evidence for non-conservative current-induced forces in the breaking of Au and Pt atomic chains. *Beilstein Journal Nanotechnoly, 6*(241), pp.2338–2344.
33. Walus, K., Karim, F. and Ivanov, A., **2009**. Architecture for an external input into a molecular QCA circuit. *Journal of Computational Electronics, 8*(1), pp.35–42.

Received: xx Xxxx xxxx. Accepted: xx Xxxx xxxx.